APL Materials

Research Update: Fast and tunable nanoionics in vertically aligned nanostructured films

Cite as: APL Mater. 5, 042304 (2017); https://doi.org/10.1063/1.4978550
Submitted: 23 November 2016 . Accepted: 27 February 2017 . Published Online: 22 March 2017

Shinbuhm Lee, and Judith L. MacManus-Driscoll

Research Update: Fast and tunable nanoionics in vertically aligned nanostructured films

Shinbuhm Lee[1,a] and Judith L. MacManus-Driscoll[2]
[1]*Department of Emerging Materials Science, Daegu Gyeongbuk Institute of Science and Technology, Daegu 42988, South Korea*
[2]*Department of Materials Science and Metallurgy, University of Cambridge, 27 Charles Babbage Road, Cambridge CB3 0FS, United Kingdom*

(Received 23 November 2016; accepted 27 February 2017; published online 22 March 2017)

This review provides the design principles to develop new nanoionic applications using vertically aligned nanostructured (VAN) thin films, incorporating two phases which self-assemble in one film. Tunable nanoionics has attracted great attention for energy and device applications, such as ion batteries, solid oxide fuel cells, catalysts, memories, and neuromorphic devices. Among many proposed device architectures, VAN films have strong potential for nanoionic applications since they show enhanced ionic conductivity and tunability. Here, we will review the recent progress on state-of-the-art nanoionic applications, which have been realized by using VAN films. In many VAN systems made by the inclusion of an oxygen ionic insulator, it is found that ions flow through the vertical heterointerfaces. The observation is consistent with structural incompatibility at the vertical heteroepitaxial interfaces resulting in oxygen deficiency in one of the phases and hence to oxygen ion conducting pathways. In other VAN systems where one of the phases is an ionic conductor, ions flow much faster within the ionic conducting phase than within the corresponding plain film. The improved ionic conduction coincides with much improved crystallinity in the ionically conducting nanocolumnar phase, induced by use of the VAN structure. Furthermore, for both cases Joule heating effects induced by localized ionic current flow also play a role for enhanced ionic conductivity. Nanocolumn stoichiometry and strain are other important parameters for tuning ionic conductivity in VAN films. Finally, double-layered VAN film architectures are discussed from the perspective of stabilizing VAN structures which would be less stable and hence less perfect when grown on standard substrates. [http://dx.doi.org/10.1063/1.4978550]

I. INTRODUCTION

Ionics has been traditionally used for long-standing energy applications,[1,2] i.e., ion batteries which rely on the ionic motion of either Li or Na;[3–10] solid oxide fuel cells based on the ionic motion of either oxygen or hydrogen;[11–14] and catalysts which use oxidation and reduction processes of O_2 or CO_2,[15–17] and so on. In these applications, compared with electronic motion, ionic motion is essentially very slow,[18] resulting in many unsolved challenges. In ion batteries, charging/discharging processes, whereby ions move from one electrode to another, take several hours. In solid oxide fuel cells, to give sufficiently fast electrolyte diffusion as well as sufficiently fast cathodic reactions, operation temperatures should be higher than ~650 °C. Such a high temperature results in the melting of metallic interconnects and leads to rapid cell degradation. In catalysts, very expensive novel metals have been used to promote oxidation and reduction processes. Therefore, for the future development of energy applications, enhancing ionic conduction near room temperature is highly desirable.

[a]Electronic mail: lee.shinbuhm@dgist.ac.kr

Recently, there have been many efforts to develop universal devices which have ionic and electronic characters, so-called ionotronics,[2] working at room temperature. Solid state ionotronic devices had not been seriously developed, since slow ion motion does not guarantee fast operation of nanosecond time scale, which is usually achieved by most conventional electronic devices. However, with the development of nanostructure fabrication techniques, device operating has been significantly fast to nanosecond time scale since ions move over the nanoscale length. Next-generation memory devices based on resistive switching (RS) phenomena have been demonstrated using ionic motion in semiconductors.[19–26] When an electric field is applied, ions move toward one electrode, and accumulate and form conducting channels, resulting in a low-resistive state of the device. When an electric field with opposite polarity is applied, the ions in the channels move back to the other electrode; therefore, the channels are dissolved and ruptured, resulting in a high-resistive state of the device. The working principle of this memory effect is highly similar to that of a neuromorphic system in the human neural network.[27,28] Therefore, ionic devices have attracted renewed interest to mimic the neuromorphic systems and to develop neuromorphic devices, so-called neuristors.

The development of next-generation memory using ionic devices also strengthens the importance of tunability of ionic conductivity. Tunable "electronic" conductivity in "conventional" memory devices enables the realization of multilevel resistance states which radically increases memory data storage capacity. In the same way, tunable ionic conductivity will enable data storage of ionic memory devices to be increased.[29,30] In addition, multilevel memory states will enable more delicate mimicking of short-term and long-term memories in the human neuromorphic system.[27,28]

II. NEW DEVICE ARCHITECTURES FOR IONIC DEVICES

To achieve tunable as well as high ion conductivity for ionic devices working near room temperature, several device architectures have been proposed as follows.

The standard way to enhance oxygen ionic conduction in oxides is the partial substitution of aliovalent rare earth cations to increase the concentration of oxygen vacancies,[11,13] as shown in Figure 1(a). Y-stabilized ZrO_2 (YSZ) and Sm-doped CeO_2 (SDC) are very well-known examples for electrolytes in solid oxide fuel cells. However, the operation temperature for reasonable ionic conduction is above ~650 °C since the thermal activation barrier for ion hopping still remains high regardless of vacancy concentration.

Recently, to enhance ionic conductivity in solid oxide fuel cells, new device architectures have been developed by using interfaces at laterally aligned heteroepitaxy films, as shown in Figure 1(b). The lateral interfaces in CaF_2/BaF_2 superlattices showed high ionic conductivity of F ions due to the overlap of space charges.[31] Lateral interfaces in superlattices of YSZ and $SrTiO_3$ show high ionic conductivity of oxygen ions.[32] However, the underlying mechanism is still under debate since the increase in conduction is much larger than the theoretical prediction.[33,34] Irrespective of high ionic conductivity, laterally aligned heteroepitaxy films are rarely practical for commercial applications. Each epitaxial layer needs to be grown carefully, one layer by another, and very long deposition times are required. More importantly, since the number of lateral interface is not large, the actual current

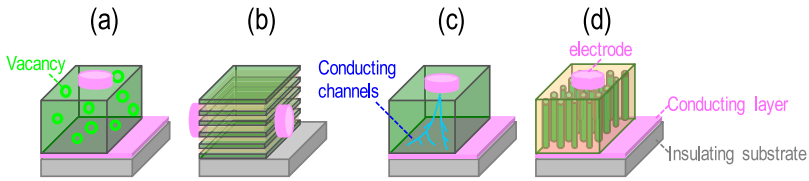

FIG. 1. Various nanostructures proposed to enhance ionic conductivity. (a) Creating oxygen vacancies by cation doping in oxide thin films. (b) Formation of fast ionic conduction channels perpendicular to the normal direction of the substrate in laterally aligned heteroepitaxy films. (c) Creating oxygen vacancies by the electric-field-induced electroforming process. (d) Formation of fast ionic conduction channels parallel to the normal direction of the substrate in vertically aligned nanostructured (VAN) films. Reproduced with permission from Lee *et al.*, Adv. Mater. **26**, 6284 (2014).

flow is not large. Finally, the ions do not flow in the perpendicular-to-substrate plane direction thus making the geometry impractical for high integration density potential for ionotronic devices.

A decrease of the film thickness into the nanoscale regime has boosted the development of ionic memory devices.[19–26,30,35] As shown in Figure 1(c), the device structures are usually composed of oxide thin films (or semiconductor thin films) with either novel metal (e.g., Au and Pt) electrodes or mobile metal (e.g., Ag or Cu) electrodes. However, most as-grown films are not sufficient to display electric-field-induced RS phenomena. The reason for this is that the concentration of actively working ions, e.g., oxygen vacancies in oxides and mobile Ag^+/Cu^+ ions in semiconductors, is insufficient for the RS phenomena to occur. Therefore, a prerequisite "electroforming" process is necessary to initiate RS phenomena.[36–38] When a high electric field, higher than operating voltages of RS phenomena, is applied to the as-grown films, oxygen vacancies (and associated conduction electrons) are suddenly generated or mobile Ag^+/Cu^+ ions are immersed into the semiconductor from the Ag/Cu electrodes through a controlled breakdown process. However, unfortunately this electroforming process causes many critical problems for reliability in memory operation.[36] The size of conducting channels ranges from a few to a few tens of nanometer.[39,40] The connection and rupture of the channels are governed by a percolating behavior,[20,25,41,42] inducing highly random device performance. Furthermore, huge current overshot occurs during the electroforming process, sometimes burning the ionic memory devices. Such critical problems encourage the development of new device architectures, which can eliminate the electroforming process and minimize the random connection of conducting channels.

Very recently, as shown in Figure 1(d), new and novel device architectures, vertically aligned nanostructured (VAN) films,[43–53] were developed to overcome several issues in conventional ionic devices as mentioned above. Basically, the development of ionic devices by using VAN films started from a similar motivation of laterally aligned heteroepitaxy films. Figure 2 shows cross-sectional and plan-view transmission electron microscopy images. In VAN films, many nanocolumns of diameter of a few tens of nanometer are embedded in a film matrix. The nanocolumns are immiscible within the matrix, so the phases are clearly separated.

Here, we will review the recent development of VAN films for state-of-the-art ionic devices. In Sec. III, to understand how to grow such a seemingly complex, while in fact, rather simple and self-assembled device architecture, we explain the growth mechanism of VAN films. Accordingly, we will also discuss the criteria of how to select appropriate matrix and nanocolumn combinations. In Sec. IV, we introduce several energy and ionic device applications of VAN films, such as memories,

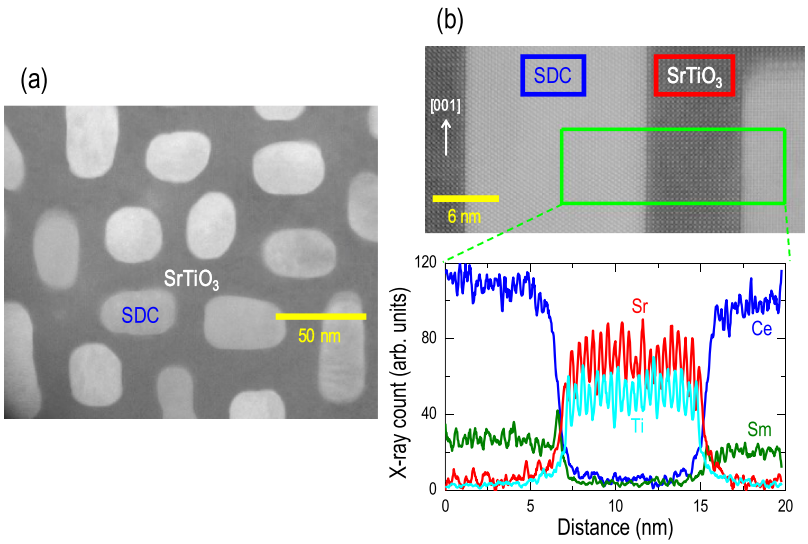

FIG. 2. (a) Plan-view and (b) Cross-sectional-view scanning transmission electron microscopy images of VAN films of Sm-doped CeO_2 (SDC) and $SrTiO_3$. Separation of SDC nanocolumns from the $SrTiO_3$ matrix is clearly visualized. Energy dispersive X-ray spectroscopy in the bottom of (b) shows the sharp interface between the SDC nanocolumns and $SrTiO_3$ matrix without significant chemical intermixing. Courtesy of Dr. Ping Lu (Sandia National Laboratory, USA).

solid oxide fuel cells, catalysts, and water splitting. In Sec. V, we discuss the origin of high ionic conductivity in VAN films. In Sec. VI, control parameters will be discussed to tune ionic conductivity in VAN films. Finally, we propose a perspective engineering technique to improve ionic devices of VAN films. Although this review might not cover all findings in this research field, we hope that it will help the readers to quickly jump into the field of ionic devices based on VAN films. If the readers are interested in other applications, such as electric and magnetic properties of VAN films, there are several reviews[54–56] and reports[57–69] which are worth reading.

III. GROWTH MECHANISMS OF VAN FILMS

The growth mechanisms of VAN films have been discussed in recent reviews.[54–56] Pulsed laser deposition (PLD) is the standard growth method of VAN films. The targets for PLD are made by mixing and pelletizing the two immiscible oxide powders, which will be matrix and nanocolumns in the VAN films. It is also possible to mix the binary oxides together, but sintering, grinding, and re-pelletizing are advised to ensure homogeneity. When a pulsed laser ablates the target in a vacuum chamber, the species are evaporated from the target to form a plume. If a heated substrate is placed within the plume, then the species adsorb on the substrate and diffuse along its surface. The composite VAN film grows via self-assembly, first by the nucleation of energetically preferred phases on the surface and then by the growth of the lowest Gibbs free energy phases in the composite. Vertical epitaxy between the growing phases is a key factor in the growth process. VAN films can either be deposited from a single target (as is most commonly and simply done) or indeed by ablating two targets with the help of an automated carousel.[70] It is important to note that epitaxial VAN films are no more complicated to grow than standard epitaxial films. From an application point of view, the challenge is, therefore, *not* any complication of the VAN structures but, instead, it is the use of PLD, just as for other epitaxial oxides. PLD is relatively costly from the point of view that it needs excimer lasers. Also it has limitations on large area growth. On the other hand, several methods could replace PLD for the industrial growth of complex oxides, namely, metal organic chemical vapor deposition, sputtering, or electron beam evaporation.

Irrespective of the simple growth mechanism of VAN films, the selection of the two phases to be grown in the VAN film is relatively straightforward and is discussed at length.[54–56] In short, one of the essential conditions which should be satisfied for high quality VAN films is *immiscibility* between the two phases. Broadly, cation sizes within the phases and the crystal structures of them should be different. For example, perovskite-fluorite, perovskite-bixbyte, and perovskite-spinel are good choices. Clear separation is also promoted if one of the phases has the same crystal structure as the substrate, enabling easy nucleation and epitaxial growth of that phase. The specific nanostructural arrangement of composite depends on the ratio of the phases as well as mismatch strains.[71]

VAN films have several merits compared to laterally aligned heteroepitaxy films, as introduced in previous reviews.[54–56] While the growth of laterally aligned heteroepitaxy films is complicated and slow due to the need for layer-by-layer growth and perfection of each layer to maintain good heteroepitaxy, VAN films can be grown in a short time since one ablation of the target releases both species simultaneously. Furthermore, epitaxy does not degrade with thickness because *vertical* epitaxy dominates the growth,[61,63,72–74] independent of the substrate. This permits entirely new strain states to be realized with elastic constants and thermal expansion constants of the phases playing strong roles. With 5-20 nm lateral dimensions of nanopillars, a huge number of vertical heterointerfaces in VAN films are formed in a short time. As described in more detail below, for ionic VAN structures, current flows either along vertical heterointerfaces or the nanocolumns, whose direction is parallel to the connection between top and bottom electrodes. Therefore, the integration density of ionic devices is much higher in VAN films.

IV. EMERGING NANOIONICS IN VAN FILMS

VAN films have shown enhanced performance for energy and ionotronic devices. In this section, we will introduce several interesting examples, such as memories using RS phenomena,[46,52] solid

oxide fuel cells,[43,47–50] and water splitting.[53] Further applications, as yet unexplored, would be entirely possible by tailoring the various properties of VAN films.

A. Resistive switching phenomena

VAN films show RS phenomena without the need for an electroforming process.[46,51,52] The central image in Figure 3 shows the resistance change in SDC-$SrTiO_3$ VAN films when an external voltage is applied. When a positive voltage is applied to the as-grown sample, the device resistance changes from low to high values. When a negative voltage is applied to the high-resistive sample, the device changes to a low-resistive state again. A similar phenomenon has also been observed in $Ba_{0.6}Sr_{0.4}TiO_3$–Sm_2O_3,[46] $BaTiO_3$–Sm_2O_3,[46] $SrTiO_3$–Sm_2O_3,[46] and Nb_2O_5–$NaNbO_3$ VAN films.[51] The on/off ratios exceed two orders of magnitude. Owing to the precisely engineered nanostructured films, the ratios are highly reproducible from one sample to another. Hence, RS phenomena occur very stably for very long cycles over 10^4 cycles.

The schematic in Figure 3 shows the physical mechanism of the RS phenomena in VAN films. The RS observed is consistent with a change of the interfacial electronic barrier, the so-called Schottky barrier, between VAN films and metal electrodes. This mechanism is very similar to the RS mechanism in thin films.[21,35] Depending on the system under study, oxygen vacancies migrate either along vertical heterointerfaces (if the film contains $SrTiO_3$, i.e., an ionically insulating nanopillar phase) or through the nanocolumns (if the film contains an ionically conducting phase). As shown in panels 1-5, when positively charged oxygen vacancies are accumulated near the interface between the VAN film and the metal electrode by the application of a negative voltage, the interfacial electronic barrier is lowered, accordingly resulting in the device resistance changing from the high to low-resistive state. On the contrary, as shown in panels 6-8, when a positive voltage is applied to the device, oxygen vacancies are repelled from the metal electrode and the interfacial electronic barrier is recovered, moving the device into the high-resistive state. Sometimes, a high-to-low resistance change occurs with the application of a positive voltage, and vice versa, as observed in $SrTiO_3$–Sm_2O_3 VAN films.[46] This

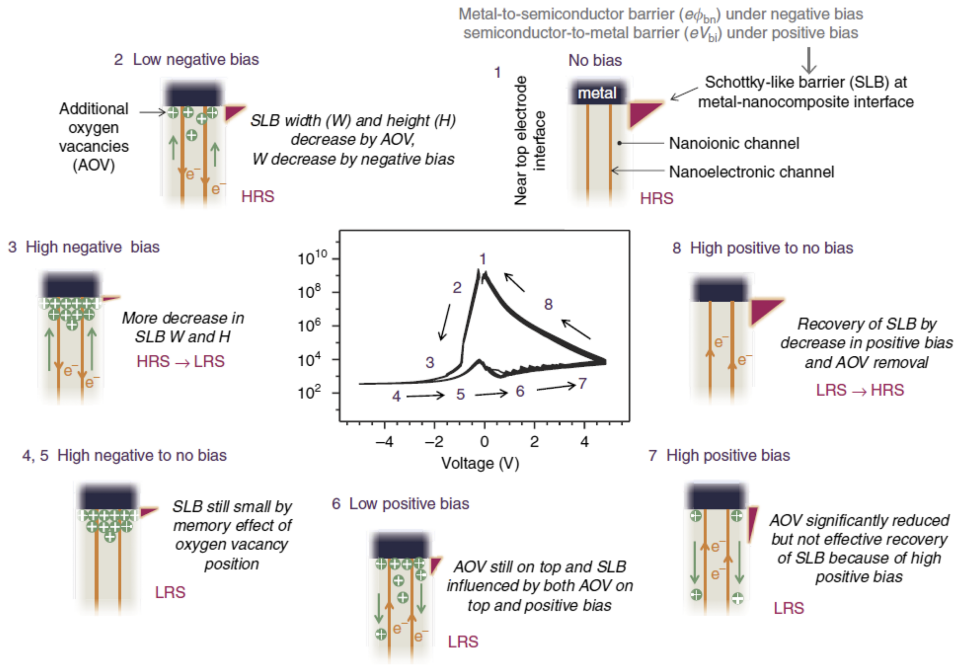

FIG. 3. (center) Resistive switching (RS) phenomena in SDC-$SrTiO_3$ VAN films. RS phenomena started without the electroforming and are very stable after harsh operation. It should be noted that the electroforming is required to initiate RS phenomena in plain films with the application of a large electric field. (surroundings) Proposed mechanism of RS phenomena in VAN films. The detailed description is noted on each figure. LRS and HRS stand for low-resistive state and high-resistive state, respectively. Reproduced with permission from Cho *et al.*, Nat. Commun. **7**, 12373 (2016).

unconventional behavior is attributed to oxygen vacancies being accumulated either near or far from the metal electrodes. A detailed explanation of these observations has been given by Lee *et al.*[75,76] and is beyond the scope of this review.

B. Solid oxide fuel cells

Figure 4 shows the measured oxygen ionic conductivity versus temperature for VAN films including YSZ and SDC, compared to YSZ films, doped CeO_2 films, and their multilayer films.[11,13,33,77–82] Enhanced ionic conductivity values by one order of magnitude or more are observed.[49,50] Enhancement of ionic conductivity values has also been observed in VAN films of YSZ and Gd-doped CeO_2.[83] Such high ionic conductivity values (in film thicknesses up to over a micron) could enable significantly decreased operation temperatures of micro solid oxide fuel cells to well below 650 °C. The origin of enhanced ionic conductivity in VAN films will be discussed in Section V.

VAN films have also been used to enhance the oxygen reduction reaction at the cathodes in solid oxide fuel cells. As shown in Figure 5, Ma *et al.*[48] showed, in the temperature range of 320–400 °C,

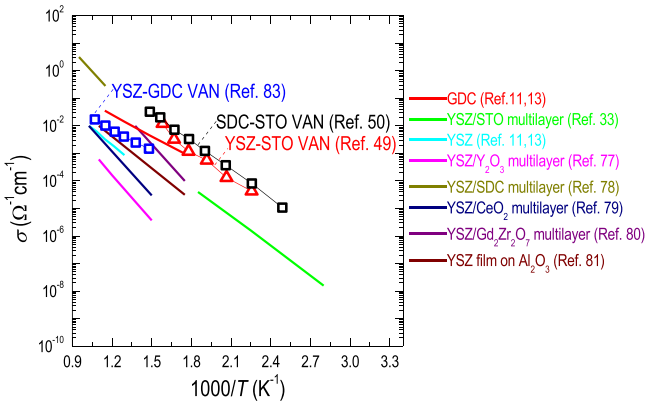

FIG. 4. Enhanced ionic conductivity of YSZ-Gd-doped CeO_2 (GDC) VAN, YSZ-$SrTiO_3$ VAN, SDC-$SrTiO_3$ VAN films, as indicated by symbols. Solid lines indicate experimental reports from plain films and laterally aligned heteroepitaxy films including YSZ and doped CeO_2.

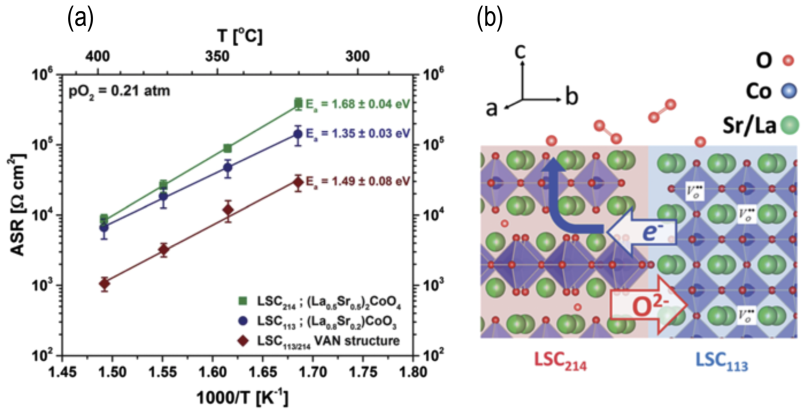

FIG. 5. (a) Temperature dependence of the area specific resistance (ASR) of oxygen surface exchange reaction on the surface of $(La_{1-x}Sr_x)CoO_3$ and $(La_{1-x}Sr_x)_2CoO_4$ plain films and that of $(La_{1-x}Sr_x)CoO_3$–$(La_{1-x}Sr_x)_2CoO_4$ VAN film measured in air. (b) Schematic model of "electronically coupled oxide heterointerfaces" made of $(La_{1-x}Sr_x)CoO_3$ and $(La_{1-x}Sr_x)_2CoO_4$. At high temperature, more oxygen vacancies and free electrons are created in the $(La_{1-x}Sr_x)CoO_3$ phase. The excess electrons are injected into the $(La_{1-x}Sr_x)_2CoO_4$ phase from $(La_{1-x}Sr_x)CoO_3$, facilitating the oxygen reduction reaction at the $(La_{1-x}Sr_x)_2CoO_4$ surface. Faster oxygen reduction reaction kinetics are expected at $(La_{1-x}Sr_x)CoO_3$–$(La_{1-x}Sr_x)_2CoO_4$ VAN films given the high density of heterointerfaces. Reproduced with permission from Ma *et al.*, J. Mater. Chem. A **3**, 207 (2015).

that oxygen reduction kinetics at $(La_{1-x}Sr_x)CoO_3$–$(La_{1-x}Sr_x)_2CoO_4$ VAN cathodes show approximately a 10-fold enhancement compared to the respective single phases of either $(La_{1-x}Sr_x)CoO_3$ or $(La_{1-x}Sr_x)_2CoO_4$. Furthermore, *in situ* scanning tunneling spectroscopy established that the $(La_{1-x}Sr_x)_2CoO_4$ domains in the VAN structure became electronically activated, by charge transfer across the interfaces with adjacent $(La_{1-x}Sr_x)CoO_3$ domains. Atomic force microscopy and X-ray photoelectron spectroscopy analyses revealed that the interfaces provide a more stable cation chemistry at the surface of $(La_{1-x}Sr_x)_2CoO_4$, compared to single phase $(La_{1-x}Sr_x)_2CoO_4$ films. Therefore, the higher reactivity of the VAN surface to the oxygen reduction reaction is attributed to enhanced electron availability for charge transfer as well as the suppression of detrimental cation segregation.

VAN films can act as interconnection layers between the electrolyte and electrode in solid oxide fuel cells. As shown in Figure 6, Yoon *et al.*[43] deposited a $Ce_{0.9}Gd_{0.1}O_{1.95}$–$La_{0.5}Sr_{0.5}CoO_3$ VAN film between a $Ce_{0.9}Gd_{0.1}O_{1.95}$ electrolyte and a $La_{0.5}Sr_{0.5}CoO_3$ cathode. The VAN structure significantly improved the overall performance of the solid oxide fuel cells by increasing the interfacial area between the electrolyte and cathode. The VAN interlayer could also act as a transition layer that improves adhesion and relieves both thermal stress and lattice strain between the cathode and the electrolyte.

C. Water splitting

VAN films of $ZnFe_2O_4$–$SrTiO_3$ have been shown to give strongly enhanced photoelectrochemical solar water oxidation.[53] As shown in Figure 7(a), the $ZnFe_2O_4$–$SrTiO_3$ VAN films yielded an enhanced photocurrent density of 0.188 mA/cm^2 at 1.23 V vs. the reversible hydrogen electrode, which was 7.9- and 2.6-fold higher than that of individual $SrTiO_3$ and $ZnFe_2O_4$ plain film cases under 1-sun illumination, respectively. Figure 7(b) shows a vertical alignment of $ZnFe_2O_4$ and $SrTiO_3$ in VAN films, which plays an important role in the separation of hole and electron and accordingly in enhanced photo-induced charge separation.

V. ORIGIN OF ENHANCED IONIC CONDUCTIVITY IN VAN FILMS

There have been many efforts to understand the enhanced ionic conductivity in VAN films. First of all, the overlap of space charge regions, which was proposed by Sata *et al.*,[31] was considered to explain enhanced F-ion conductivity in CaF_2/BaF_2 systems. However, since the space charge region of heavily doped ionic conductors, such as YSZ and doped CeO_2, is very narrow, i.e., 1 nm,[84] the overlap of space charge regions is not possible for typical VAN films which contain nanocolumns of diameter and pitch of 10-20 nm. By considering many VAN systems, two possible mechanisms have been proposed, as discussed below.

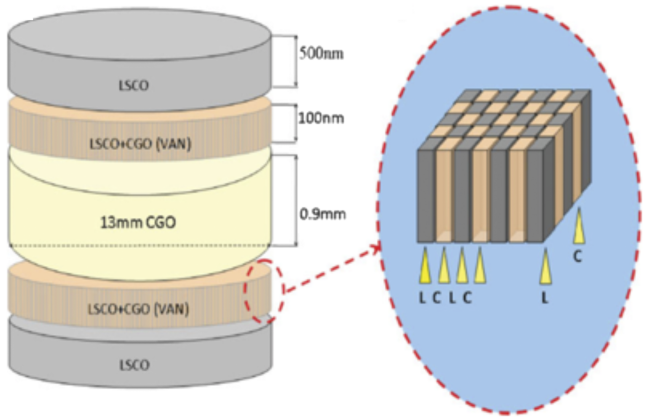

FIG. 6. Schematic of $Ce_{0.9}Gd_{0.1}O_{1.95}$–$La_{0.5}Sr_{0.5}CoO_3$ VAN interconnect layer between $Ce_{0.9}Gd_{0.1}O_{1.95}$ electrolyte and $La_{0.5}Sr_{0.5}CoO_3$ cathode. C and L denote $Ce_{0.9}Gd_{0.1}O_{1.95}$ and $La_{0.5}Sr_{0.5}CoO_3$, respectively. Reproduced with permission from Yoon *et al.*, Adv. Funct. Mater. **19**, 3868 (2009).

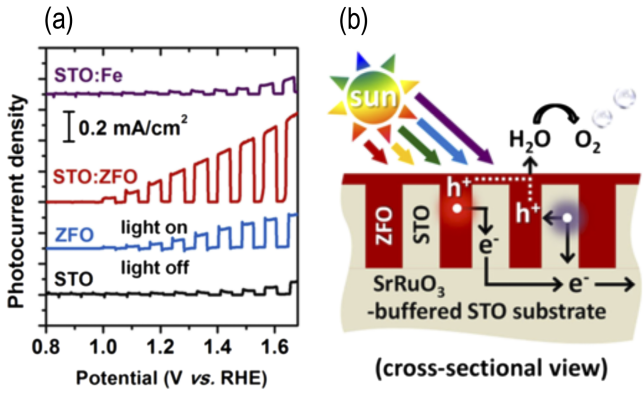

FIG. 7. Photoelectrochemical solar water oxidation properties in $SrTiO_3$–$ZnFe_2O_4$ VAN films. (a) Photocurrent density curve of 2% Fe-doped $SrTiO_3$, $SrTiO_3$, $ZnFe_2O_4$ plain films and $SrTiO_3$–$ZnFe_2O_4$ VAN films in 1M NaOH solution under chopped 1-sun illumination. (b) Schematic illustrations of electron-hole separation along $SrTiO_3$ and $ZnFe_2O_4$ phases, respectively. Reproduced with permission from Cho *et al.*, Chem. Mater. **28**, 3017 (2016).

A. Oxygen deficiency at vertical heterointerfaces due to structural incompatibility

To understand the physical mechanism(s) of ion conductivity enhancement, the spatial distribution of ionic transport in vertical channels in VAN films was measured using atomic force microscopy (AFM). Figures 8(a) and 8(b) show the first observation of conducting AFM in VAN films of $BiFeO_3$–$CoFe_2O_4$.[44,45] The 2 nm area at the vertical heterointerfaces showed brighter colors, indicating that high electronic conduction was localized at those interfaces. Further inves-

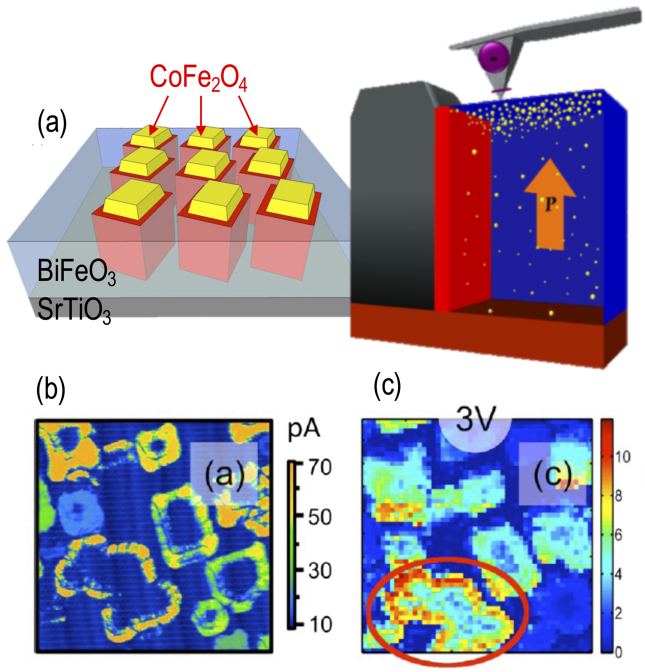

FIG. 8. Ion transport pathways localized at heterointerfaces in $BiFeO_3$–$CoFe_2O_4$ VAN films. (a) Schematics show that VAN films are composed of $CoFe_2O_4$ nanocolumns and $BiFeO_3$ matrix. To detect ion transport pathways, a cantilever in conducting atomic force microscopy (AFM) was used on the film surface in a contact mode. (b) While current does not flow through both nanocolumns and matrix, there is current flow at vertical heterointerfaces when a voltage is applied. The current map over a wide surface area indicates that vertical heterointerfaces are electronically conducting. (c) When electrochemical AFM is undertaken on the film surface, ion transport is also activated at the vertical heterointerfaces. Reproduced with permission from Hsieh *et al.*, ACS Nano **7**, 8627 (2013).

tigations were performed using electrochemical AFM, which can detect ion motion. The operating principle is that current-voltage curves measured by conducting AFM show hysteresis loops when ionic flow is responsible. Figure 8(c) shows the mapping of the calculated area of the hysteretic current-voltage curves at each spatial point.[44,45] As the color changes from blue to red, the ionic effects are stronger. The red-colored area, indicating high ion conduction, mainly appears at the vertical heterointerfaces and is consistent with the electrically conducting area measured by conducting AFM.

Nanoscopic tools equipped with transmission electron microscopy (TEM) have been employed to obtain further information about ionic conduction enhancement. As shown in Figure 9, electron energy loss spectroscopy has been used to investigate elemental chemical concentrations at vertical heterointerfaces.[46] In $SrTiO_3$–Sm_2O_3 VAN films, the oxygen content was found to be deficient compared with the theoretical predictions, indicating the existence of oxygen vacancies at vertical heterointerfaces. This deficiency is consistent with oxygen vacancies induced by interface structural incompatibility[85] (i.e., between different perovskite $SrTiO_3$ ($Pm\bar{3}m$) and bixbyte Sm_2O_3 ($Ia\bar{3}$)). Using TEM, a similar structural incompatibility was also observed at the vertical heterointerfaces in $BiFeO_3$–$CoFe_2O_4$ VAN films.[44] This interface was further investigated

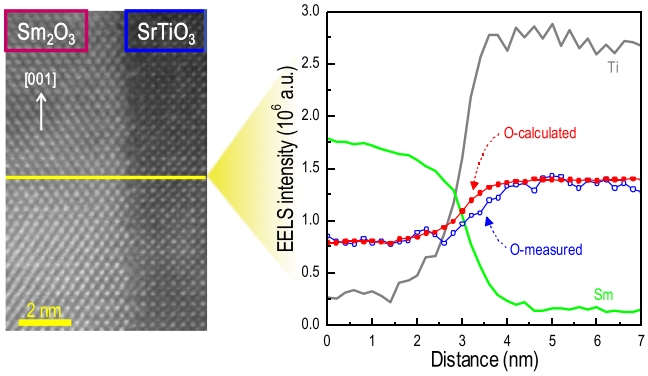

FIG. 9. Oxygen deficiency at vertical heterointerfaces in $SrTiO_3$–Sm_2O_3 VAN films. Electron energy loss spectroscopy (right) was measured along the yellow line in high-angle annular dark field image equipped with scanning transmission electron microscopy (left). It should be noted that the measured oxygen intensity is lower than the theoretically predicted one in the vertical heterointerface regions. Reproduced with permission from Lee *et al.*, Adv. Mater. **26**, 6284 (2014).

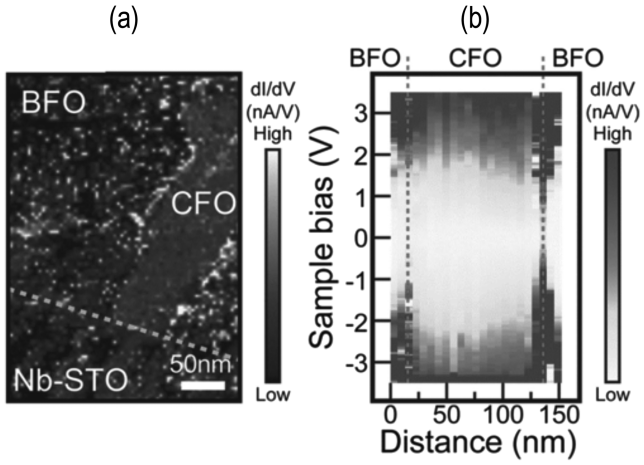

FIG. 10. Cross-sectional scanning tunneling microscopy and spectroscopy near the interface of $BiFeO_3$–$CoFe_2O_4$ VAN films. (a) Cross-sectional spectroscopic image of the epitaxial hetero-structure. The dotted line indicates the position of the interface between the nanostructures and the substrate. (b) A reconstructed band alignment to reveal the variation of the bandgap across the $BiFeO_3$/$CoFe_2O_4$ interface. Reproduced with permission from Hsieh *et al.*, Adv. Mater. **24**, 4564 (2012).

by cross-sectional scanning tunneling microscopy and spectroscopy, as shown in Figure 10. The bandgap was found to shrink across the $BiFeO_3/CoFe_2O_4$ interfaces. The interface conduction was enhanced because the atomic discontinuity added interface states and/or modified electronic structure.

B. Improved crystallinity of ionic conductors

When ionic conducting nanocolumns are formed in VAN films, their improved crystallinity plays an important role in producing enhanced ionic conductivity. The ionic conduction of SDC-$SrTiO_3$ VAN films has been measured by electrochemical AFM. As shown in Figure 11, it was found that the ionic conducting regions were observed only *within* SDC nanocolumns and *not* at the vertical heterointerfaces.[50] This result is in contrast with activated ionic transport occurred at the vertical heteroepitaxial $BiFeO_3$–$CoFe_2O_4$ VAN interfaces, as mentioned in Section V A. This begs the question about what is the difference between SDC–$SrTiO_3$ and $BiFeO_3$–$CoFe_2O_4$ VAN films. One clear difference is that SDC is strongly ionically conducting while $SrTiO_3$, $BiFeO_3$, and $CoFe_2O_4$ are ionically insulating, at least below 650 °C. In other words, ionic conduction within SDC is dominant over any interface induced ionic conduction whether it is in $SrTiO_3$ or $BiFeO_3$.

A possible explanation for the enhanced ionic conductivity in VAN films incorporating ionic conductors is improved crystallinity.[49,50] When plain heteroepitaxial SDC films are of micrometer-scale, as required for industrial requirements, they have many strain-relaxation related structural defects. These are known to hinder oxygen ionic transport.[86,87] On the other hand, in VAN films comprising ionically conducting SDC nanopillars, the crystallinity of the SDC phase is much enhanced.[50,56] The reason for the enhanced crystallinity in VAN films is related to the large area vertical heteroepitaxy along many interfaces,[73] contrasting with the single interface formed in a planar film. Full understanding of the uniform strain and defect reduction requires further basic studies.

C. Joule heating effects

Joule heating effects might play an important role to enhance ionic conductivity in VAN films. When ions flow along vertical heterointerfaces, current is localized in a very narrow interfacial area of a few nanometers. Similarly, the current flow, induced by ion flow along nanocolumns of ionic conductors, is also localized in a few tens of nanometers. It is widely accepted that the current flow along such a narrow pathway results in Joule heating effects.[88,89] This thermal effect accelerates ion migration in VAN films. Lee *et al.*[46] used finite element methods to understand Joule heating effects for ionic motion when ions flow along vertical heterointerfaces in VAN films. Figure 12 shows a simplified schematic model of $SrTiO_3$–Sm_2O_3 VAN films, which show the RS phenomena. When ions are assumed to mainly flow through 2-nm-wide heterointerfaces, measured transient times τ for high-to-low resistive switching could be well fit with the consideration of Joule heating effects.

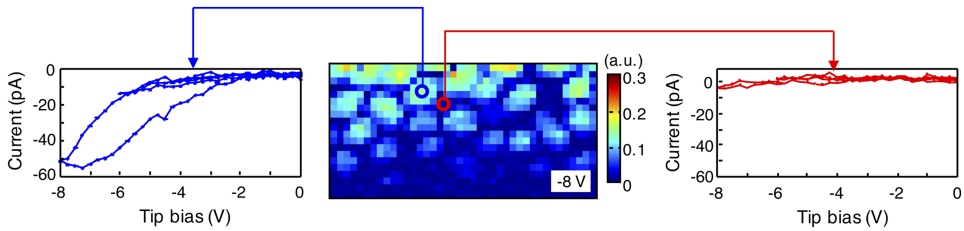

FIG. 11. Electrochemical AFM image of SDC-$SrTiO_3$ VAN films. Electrochemical AFM undertaken on the film surface indicates that ion transport is localized within the SDC nanocolumns. While a first order reversal curve of the current-voltage curve at SDC nanocolumns (left) has a hysteresis behavior, there is no current flow in $SrTiO_3$ matrix (right), indicating that ion transport is significantly activated only in the SDC nanocolumns. Reproduced with permission from Yang *et al.*, Nat. Commun. **6**, 8588 (2015).

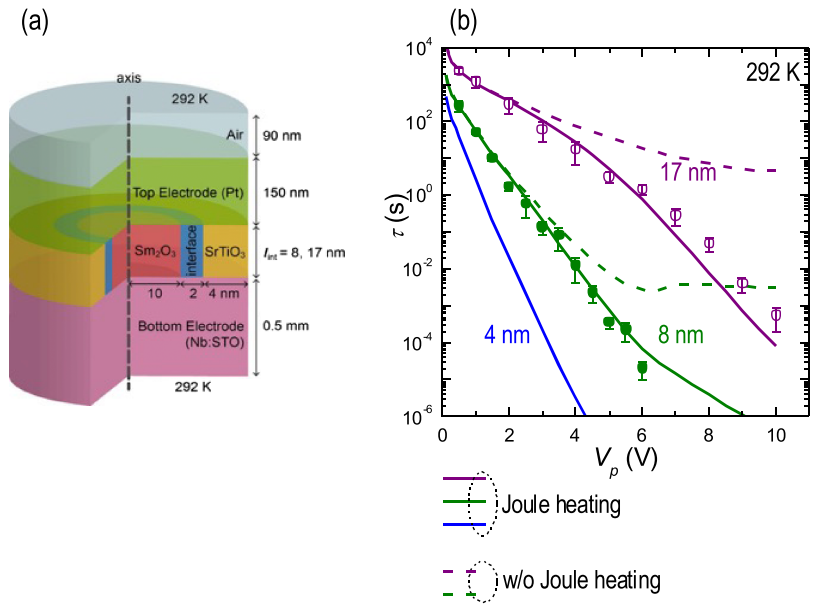

FIG. 12. Joule heating assisted ion conducting enhancement. (a) Schematic represents a simplified VAN nanostructure of $SrTiO_3$–Sm_2O_3. The vertical heterointerfaces between $SrTiO_3$ and Sm_2O_3 are assumed to be electronically and ionically conducting. (b) Transient times τ for high-to-low resistive switching were measured when various amplitudes V_p of voltage pulses were applied. When Joule heating effect is considered, measured τ-values are well fit with theoretical estimations, as indicated by solid lines. Reproduced with permission from Lee *et al.*, Adv. Mater. **26**, 6284 (2014).

VI. TUNABLE IONIC CONDUCTIVITY

A. Engineering nanocolumn stoichiometry

The RS phenomenon is tunable in as-grown VAN films since it occurs without any electroforming process.[46,52] As shown in Figure 13, in SDC-$SrTiO_3$ VAN films,[52] the resistance value in the low-resistive state decreased with an increase of the atomic ratio of Sm to Ce, up to 20%. This trend is highly consistent with Sm concentration dependence of ionic conductivity in SDC, indicating that the RS phenomena in SDC-$SrTiO_3$ VAN films occur homogeneously in SDC nanocolumns. The low-resistive values also depend on the growth rate of VAN films. A slow (fast) growth rate increases (reduces) the diameter of nanocolumns since the nucleation time is sufficient (insufficient). Slow growth rates give improved crystallinity, as expected, which reduces the low-resistive state and hence leads to highly reproducible on-off resistance ratios ($\sim 10^4$).

B. Strain induced by strain-controlling phase

There have been many efforts to find control parameters to tune the ionic conductivity in VAN films. Strain control of a matrix phase using stiff nanocolumns is one of the effective control parameters.[61,73,90,91] Lee *et al.* used lanthanide series binary oxides (RE_2O_3, RE = Sm, Eu, Gd, Dy, and Er) as the strain-controlling phase to enhance the ionic conductivity of $SrZrO_3$ in $SrZrO_3$–RE_2O_3 VAN films.[47] Sm_2O_3, Eu_2O_3, Gd_2O_3, Dy_2O_3, and Er_2O_3 have the same crystal structure and space group of $Ia\bar{3}$, but the lattice constant changes from 10.92 to 10.55 Å across the series. Accordingly, the strain coupling between $SrZrO_3$ and RE_2O_3 increases the lattice constant of $SrZrO_3$ for Er_2O_3 to Sm_2O_3, as confirmed by X-ray diffraction. Hence, the vertical tensile strain in $SrZrO_3$ was maximized when Sm_2O_3 was used as the strain-controlling phase. Figure 14 shows the measured ionic conductivity of $SrZrO_3$–RE_2O_3 VAN films. The ionic conductivity was enhanced by more than one order of magnitude in $SrZrO_3$–Sm_2O_3 compared to $SrZrO_3$–Er_2O_3 VAN films, which is consistent with the trend of tensile strain in $SrZrO_3$ driven by the stiffer RE_2O_3 strain-controlling phase.

Although this review mainly focuses on nanoionics in VAN films, it is worth mentioning that strain has been also employed as a critical parameter to tune ionic conductivity in laterally aligned heteroepitaxy films as well as in plain films.[32,79,82,85,92–98] Tensile strain increases the interatomic distance

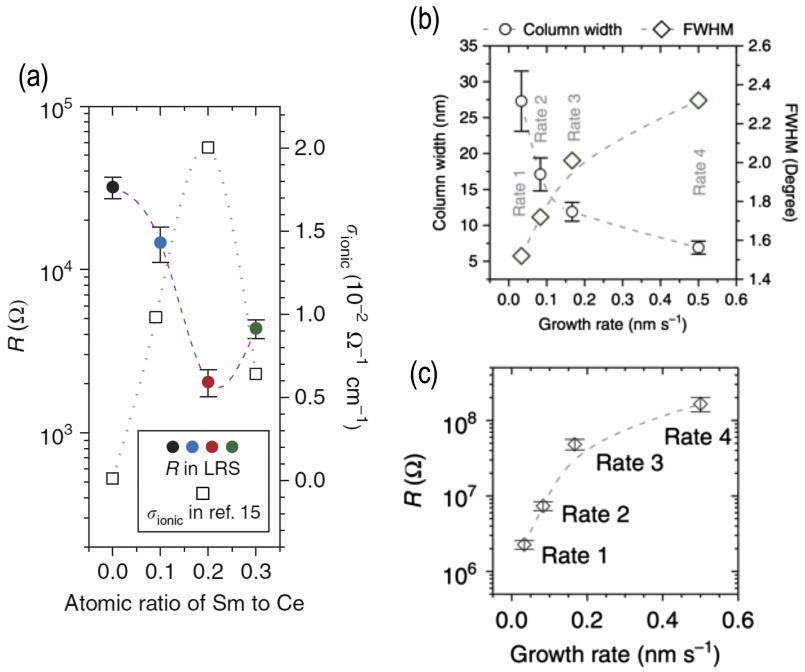

FIG. 13. Tunable RS phenomena in SDC-$SrTiO_3$ VAN films. (a) Effect of the atomic ratio of Sm/Ce on the low-resistive state. (b) Effect of the growth rate on column width and full width half maximum of X-ray diffraction ω-rocking curves. (c) Corresponding growth rate dependence of the high-resistive state. Reproduced with permission from Cho *et al.*, Nat. Commun. **7**, 12373 (2016).

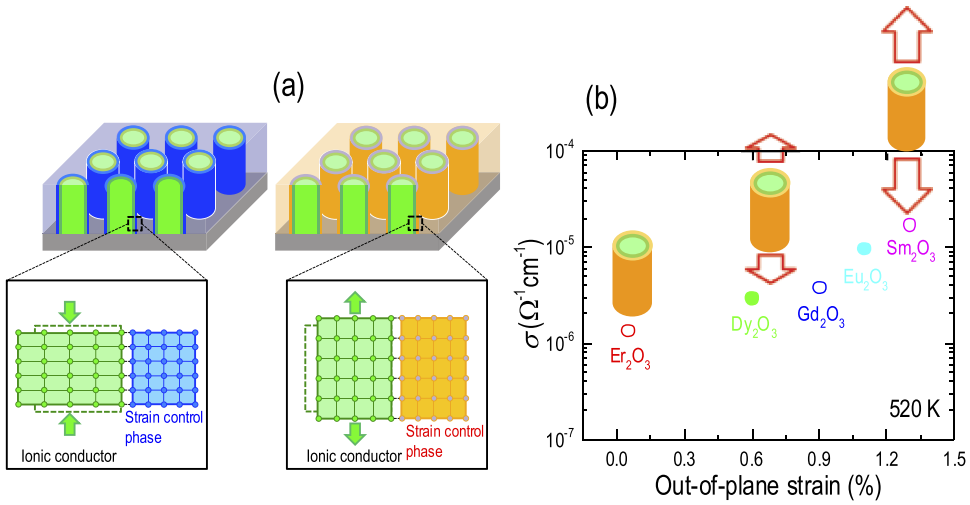

FIG. 14. Strain effect of ion transport in $SrZrO_3$–RE_2O_3 (RE = Sm, Eu, Gd, Dy, and Er) VAN films. (a) Schematic representation of the compressive (left) and tensile (right) strains in the $SrZrO_3$ ionic conductor, induced by strain-controlling RE_2O_3 nanocolumns embedded in $SrZrO_3$. (b) With an increase of tensile strain from Er_2O_3 to Sm_2O_3, the ionic conductivity of $SrZrO_3$ is systematically enhanced. Reproduced with permission from Lee *et al.*, Adv. Funct. Mater. **25**, 4328 (2015).

and weakens the atomic bonding strength;[85] therefore, the ionic conductivity of oxygen vacancies increases accordingly. A huge enhancement of ionic conductivity was observed in YSZ-$SrTiO_3$ laterally aligned heteroepitaxial films since the YSZ phase was elongated by the $SrTiO_3$ substrate with 7.5% tensile strain.[32] The ionic conductivity of the YSZ layer is also tunable in superlattices with Y_2O_3, Lu_2O_3, and Sc_2O_3.[77,92] The ionic conductivity increased with tensile strain and decreased with compressive strain. The strain state of $SrCoO_x$ thin films was controlled by systematically

changing the lattice constant of the perovskite substrates ($(LaAlO_3)_{0.3}$–$(SrAl_{0.5}Ta_{0.5}O_3)_{0.7}$, $SrTiO_3$, pseudo-cubic $DyScO_3$, pseudo-cubic $GdScO_3$, and $KTaO_3$).[95] The additional oxygen vacancies created through tensile strain enhanced the cobaltite's catalytic activity toward the oxygen evolution reaction by over an order of magnitude.[94] The surface oxygen exchange kinetics of La_2NiO_{4+d} was found to increase with a decrease of film thickness.[93] This is consistent with the increase of volumetric strain decreasing the formation energy of interstitial oxygen.

While the ionic behavior of most oxides is activated with tensile strain, it should be noted that in a few cases it is enhanced by a compressive strain. Petrie *et al.* found that compressive strain could significantly enhance oxygen reduction and oxygen evolution reactions of $LaNiO_3$ thin films.[97] This unique behavior was understood by a strain-induced splitting of the e_g orbitals, which can customize orbital asymmetry at the surface, analogous to strain-induced shifts in the *d*-band center of noble metals relative to the Fermi level. In noble metals, such a splitting can dramatically affect catalytic activity. Therefore, it is true that strain is a universal control parameter to tune the ionic conductivity, irrespective of the device architecture. However, further studies on the strain-dependence of the ionic behavior should be addressed to establish a unified mechanism.

VII. ENGINEERING VAN FILMS FOR HIGHER IONIC CONDUCTIVITY

The formation of very high quality VAN films is first controlled by materials' selection (as mentioned previously, the two phases in the film should be immiscible). However, an additional requirement is that at least one (but preferably both) of the phases should have good epitaxy with the substrate. When the epitaxy conditions of both phases to the substrate are *not* fulfilled, insertion of a templating VAN film is beneficial. Figure 15 shows YSZ-$SrTiO_3$ VAN films grown on $SrTiO_3$ with an SDC-$SrTiO_3$ templating VAN layer. When YSZ-$SrTiO_3$ VAN films are directly deposited on $SrTiO_3$ substrates, the YSZ phase has poor crystallinity due to *both* the large lattice mismatch of 7.5% between YSZ and $SrTiO_3$ *and* the different structural forms (fluorite and perovskite). On the other hand, in the SDC-$SrTiO_3$ templating VAN layer, the SDC has very good crystallinity despite it being similarly astructural with $SrTiO_3$ (again fluorite and perovskite, respectively). This is because the lattice mismatch between SDC and STO is low at 1.7%. Then when the upper YSZ-$SrTiO_3$ layer is grown on the templating SDC-$SrTiO_3$ layer, even though the lattice mismatch between YSZ and SDC is relatively high (5.5%), high quality epitaxial growth is enabled by them being isostructural. Hence, a perfect VAN structure is engineered using the double composite by exploiting first the *combination* of close lattice match of dissimilar structures (SDC on $SrTiO_3$) and then the isostructural crystal structure matching of dissimilar lattice parameter structures (YSZ on SDC). Most importantly, no special growth conditions are required to create a very high quality double composite structure, i.e., it is easily achieved over a wide range of conditions.

More interestingly, the ionic conductivity of YSZ nanocolumns in double-layer VAN films is much enhanced, compared with YSZ nanocolumns in the single-layer VAN films. This can be attributed to the improved crystallinity of YSZ in the presence of the templating SDC nanocolumns. This novel VAN templating method giving rise to double composites will significantly expand the

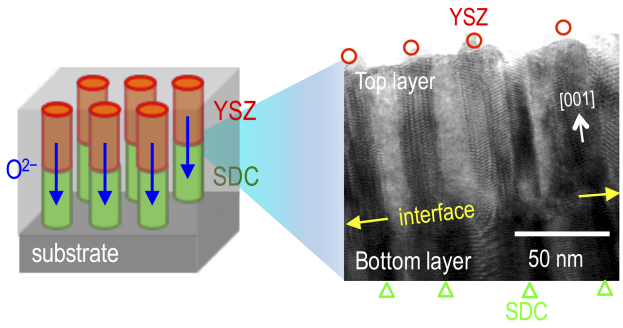

FIG. 15. Growth of YSZ-$SrTiO_3$ VAN films on $SrTiO_3$ using SDC-$SrTiO_3$ VAN templating layers. Cross section transmission electron microscopy image shows that YSZ nanocolumns (red circles) are positioned directly on SDC nanocolumns (green triangles). Reproduced with permission from Lee *et al.*, Nano Lett. **15**, 7362 (2015).

selection of compositions which can be grown for tunable ionic devices and for other applications also.

In conclusion, VAN films are powerful candidate thin film forms for a wide range of energy and ionic devices. To overcome current issues in energy materials which are hampered by slow ionic motion, VAN films have been demonstrated to give strongly enhanced performance, both in solid oxide fuel cells and in water splitting. In addition, VAN films show electroforming-free RS phenomena with improved performance in terms of stability, high on-off ratios, endurance, and reproducibility. Such films are applicable for next-generation memory and neuromorphic devices. VAN films have high ionic conductivity either at vertical interface boundaries or, in the case of films containing ionic nanocolumns, within the ionic nanocolumns themselves. Furthermore, the ionic conductivity is tunable by simply engineering the doping concentration and growth rate of the nanocolumns. Although VAN films have a great potential for ionic devices, the research is still in infancy. Further research will accelerate the tremendous applications of VAN films for a variety of new ionic devices and energy materials.

ACKNOWLEDGMENTS

We would like to appreciate Dr. Ping Lu (Sandia National Laboratory, USA) for his microscopy images. This work was supported by DGIST start-up fund (No. 2017010038) and DGIST R&D Program of the Ministry of Science (No. 2017010120). JLM-D acknowledges support from EPSRC Grant No. EP/N004272/1 and Leverhulme Grant No. RPG-2015-017.

[1] J. Maier, Nat. Mater. **4**(11), 805–815 (2005).
[2] S. V. Kalinin and N. A. Spaldin, Science **341**(6148), 858–859 (2013).
[3] J.-M. Tarascon and M. Armand, Nature **414**(6861), 359–367 (2001).
[4] P. G. Bruce, B. Scrosati, and J.-M. Tarascon, Angew. Chem., Int. Ed. **47**(16), 2930–2946 (2008).
[5] M. Armand and J.-M. Tarascon, Nature **451**(7179), 652–657 (2008).
[6] J. B. Goodenough and Y. Kim, Chem. Mater. **22**(3), 587–603 (2010).
[7] Z. Yang, J. Zhang, M. C. W. Kintner-Meyer, X. Lu, D. Choi, J. P. Lemmon, and J. Liu, Chem. Rev. **111**(5), 3577–3613 (2011).
[8] B. Dunn, H. Kamath, and J.-M. Tarascon, Science **334**(6058), 928–935 (2011).
[9] G. Crabtree, E. Kócs, and L. Trahey, MRS Bulletin **40**(12), 1067–1078 (2015).
[10] M. R. Palacín and A. de Guibert, Science **351**(6273), 1253292 (2016).
[11] E. D. Wachsman and K. T. Lee, Science **334**(6058), 935–939 (2011).
[12] Q. Van Overmeere, K. Kerman, and S. Ramanathan, Nano Lett. **12**(7), 3756–3760 (2012).
[13] E. Wachsman, T. Ishihara, and J. Kilner, MRS Bulletin **39**(9), 773–779 (2014).
[14] Y. Zhou, X. Guan, H. Zhou, K. Ramadoss, S. Adam, H. Liu, S. Lee, J. Shi, M. Tsuchiya, D. D. Fong, and S. Ramanathan, Nature **534**(7606), 231–234 (2016).
[15] H. Jeen, W. S. Choi, M. D. Biegalski, C. M. Folkman, I.-C. Tung, D. D. Fong, J. W. Freeland, D. Shin, H. Ohta, M. F. Chisholm, and H. N. Lee, Nat. Mater. **12**(11), 1057–1063 (2013).
[16] K. H. L. Zhang, P. V. Sushko, R. Colby, Y. Du, M. E. Bowden, and A. Chambers, Nat. Commun. **5**, 7 (2014).
[17] M. H. Shao, Q. W. Chang, J. P. Dodelet, and R. Chenitz, Chem. Rev. **116**(6), 3594–3657 (2016).
[18] J. C. Dyre, P. Maass, B. Roling, and D. L. Sidebottom, Rep. Prog. Phys. **72**(4), 046501 (2009).
[19] D. B. Strukov, G. S. Snider, D. R. Stewart, and R. S. Williams, Nature **453**(7191), 80–83 (2008).
[20] S. C. Chae, J. S. Lee, S. Kim, S. B. Lee, S. H. Chang, C. Liu, B. Kahng, H. Shin, D.-W. Kim, C. U. Jung, S. Seo, M.-J. Lee, and T. W. Noh, Adv. Mater. **20**(6), 1154 (2008).
[21] A. Sawa, Mater. Today **11**(6), 28–36 (2008).
[22] J. Borghetti, G. S. Snider, P. J. Kuekes, J. J. Yang, D. R. Stewart, and R. S. Williams, Nature **464**(7290), 873–876 (2010).
[23] D. S. Jeong, R. Thomas, R. S. Katiyar, J. F. Scott, H. Kohlstedt, A. Petraru, and C. S. Hwang, Rep. Prog. Phys. **75**(7), 076502 (2012).
[24] J. J. S. Yang, D. B. Strukov, and D. R. Stewart, Nat. Nanotechnol. **8**(1), 13–24 (2013).
[25] J. S. Lee, S. Lee, and T. W. Noh, Appl. Phys. Rev. **2**(3), 031303 (2015).
[26] D. S. Jeong, K. M. Kim, S. Kim, B. J. Choi, and C. S. Hwang, Adv. Electron. Mater. **2**(9), 1600090 (2016).
[27] T. Hasegawa, T. Ohno, K. Terabe, T. Tsuruoka, T. Nakayama, J. K. Gimzewski, and M. Aono, Adv. Mater. **22**(16), 1831–1834 (2010).
[28] M. D. Pickett, G. Medeiros-Ribeiro, and R. S. Williams, Nat. Mater. **12**(2), 114–117 (2013).
[29] S. C. Chae, J. S. Lee, W. S. Choi, S. B. Lee, S. H. Chang, H. Shin, B. Kahng, and T. W. Noh, Appl. Phys. Lett. **95**(9), 093508 (2009).
[30] M.-J. Lee, C. B. Lee, D. Lee, S. R. Lee, M. Chang, J. H. Hur, Y.-B. Kim, C.-J. Kim, D. H. Seo, S. Seo, U.-I. Chung, I.-K. Yoo, and K. Kim, Nat. Mater. **10**(8), 625–630 (2011).
[31] N. Sata, K. Eberman, K. Eberl, and J. Maier, Nature **408**(6815), 946–949 (2000).
[32] J. Garcia-Barriocanal, A. Rivera-Calzada, M. Varela, Z. Sefrioui, E. Iborra, C. Leon, S. J. Pennycook, and J. Santamaria, Science **321**(5889), 676–680 (2008).

[33] X. Guo, Science **324**(5926), 465 (2009).
[34] J. Garcia-Barriocanal, A. Rivera-Calzada, M. Varela, Z. Sefrioui, E. Iborra, C. Leon, S. J. Pennycook, and J. Santamaria, Science **324**(5926), 465 (2009).
[35] J. J. Yang, M. D. Pickett, X. Li, D. A. A. Ohlberg, D. R. Stewart, and R. S. Williams, Nat. Nanotechnol. **3**(7), 429–433 (2008).
[36] J. J. Yang, F. Miao, M. D. Pickett, D. A. A. Ohlberg, D. R. Stewart, C. N. Lau, and R. S. Williams, Nanotechnology **20**(21), 215201 (2009).
[37] S. B. Lee, H. K. Yoo, S. H. Chang, L. G. Gao, B. S. Kang, M.-J. Lee, C. J. Kim, and T. W. Noh, Appl. Phys. Lett. **98**(5), 053503 (2011).
[38] S. B. Lee, H. K. Yoo, K. Kim, J. S. Lee, Y. S. Kim, S. Sinn, D. Lee, B. S. Kang, B. Kahng, and T. W. Noh, Nanotechnology **23**(31), 315202 (2012).
[39] D.-H. Kwon, K. M. Kim, J. H. Jang, J. M. Jeon, M. H. Lee, G. H. Kim, X.-S. Li, G.-S. Park, B. Lee, S. Han, M. Kim, and C. S. Hwang, Nat. Nanotechnol. **5**(2), 148–153 (2010).
[40] G.-S. Park, Y. B. Kim, S. Y. Park, X. S. Li, S. Heo, M.-J. Lee, M. Chang, J. H. Kwon, M. Kim, U.-I. Chung, R. Dittmann, R. Waser, and K. Kim, Nat. Commun. **4**, 2382 (2013).
[41] J. S. Lee, S. B. Lee, S. H. Chang, L. G. Gao, B. S. Kang, M.-J. Lee, C. J. Kim, T. W. Noh, and B. Kahng, Phys. Rev. Lett. **105**(20), 205701 (2010).
[42] S. B. Lee, J. S. Lee, S. H. Chang, H. K. Yoo, B. S. Kang, B. Kahng, M.-J. Lee, C. J. Kim, and T. W. Noh, Appl. Phys. Lett. **98**(3), 033502 (2011).
[43] J. Yoon, S. Cho, J.-H. Kim, J. Lee, Z. Bi, A. Serquis, X. Zhang, A. Manthiram, and H. Wang, Adv. Funct. Mater. **19**(24), 3868–3873 (2009).
[44] Y.-H. Hsieh, J.-M. Liou, B.-C. Huang, C. W. Liang, Q. He, Q. Zhan, Y.-P. Chiu, Y. C. Chen, and Y. H. Chu, Adv. Mater. **24**(33), 4564–4568 (2012).
[45] Y.-H. Hsieh, E. Strelcov, J.-L. Liou, C.-Y. Shen, Y.-C. Chen, S. V. Kalinin, and Y.-H. Chu, ACS Nano **7**(10), 8627–8633 (2013).
[46] S. Lee, A. Sangle, P. Lu, A. Chen, W. Zhang, J. S. Lee, H. Wang, Q. Jia, and J. L. MacManus-Driscoll, Adv. Mater. **26**(36), 6284–6289 (2014).
[47] S. Lee, W. Zhang, F. Khatkhatay, Q. Jia, H. Wang, and J. L. MacManus-Driscoll, Adv. Funct. Mater. **25**(27), 4328–4333 (2015).
[48] W. Ma, J. J. Kim, N. Tsvetkov, T. Daio, Y. Kuru, Z. Cai, Y. Chen, K. Sasaki, H. L. Tuller, and B. Yildiz, J. Mater. Chem. A **3**(1), 207–219 (2015).
[49] S. Lee, W. Zhang, F. Khatkhatay, H. Wang, Q. Jia, and J. L. MacManus-Driscoll, Nano Lett. **15**(11), 7362–7369 (2015).
[50] S. M. Yang, S. Lee, J. Jian, W. Zhang, P. Lu, Q. Jia, H. Wang, T. W. Noh, S. V. Kalinin, and J. L. MacManus-Driscoll, Nat. Commun. **6**, 8588 (2015).
[51] L. Li, L. Lu, Z. Wang, Y. Li, Y. Yao, D. Zhang, G. Yang, J. Yao, D. Viehland, and Y. Yang, Sci. Rep. **5**, 9229 (2015).
[52] S. Cho, C. Yun, S. Tappertzhofen, A. Kursumovic, S. Lee, P. Lu, Q. Jia, M. Fan, J. Jian, H. Wang, S. Hofmann, and J. L. MacManus-Driscoll, Nat. Commun. **7**, 12373 (2016).
[53] S. Cho, J.-W. Jang, L. Li, J. Jian, H. Wang, and J. L. MacManus-Driscoll, Chem. Mater. **28**(9), 3017–3023 (2016).
[54] J. L. MacManus-Driscoll, Adv. Funct. Mater. **20**(13), 2035–2045 (2010).
[55] A. Chen, Z. Bi, Q. Jia, J. L. MacManus-Driscoll, and H. Wang, Acta Mater. **61**(8), 2783–2792 (2013).
[56] J. L. MacManus-Driscoll, A. Suwardi, and H. Wang, MRS Bulletin **40**(11), 933–942 (2015).
[57] O. I. Lebedev, J. Verbeeck, G. Van Tendeloo, O. Shapoval, A. Belenchuk, V. Moshnyaga, B. Damashcke, and K. Samwer, Phys. Rev. B **66**(10), 104421 (2002).
[58] H. Zheng, J. Wang, S. E. Lofland, Z. Ma, L. Mohaddes-Ardabili, T. Zhao, L. Salamanca-Riba, S. R. Shinde, S. B. Ogale, F. Bai, D. Viehland, Y. Jia, D. G. Schlom, M. Wuttig, A. Roytburd, and R. Ramesh, Science **303**(5658), 661–663 (2004).
[59] H. Zheng, F. Straub, Q. Zhan, P.-L. Yang, W.-K. Hsieh, F. Zavaliche, Y.-H. Chu, U. Dahmen, and R. Ramesh, Adv. Mater. **18**(20), 2747–2752 (2006).
[60] S. Kang, A. Goyal, J. Li, A. A. Gapud, P. M. Martin, L. Heatherly, J. R. Thompson, D. K. Christen, F. A. List, M. Paranthaman, and D. F. Lee, Science **311**(5769), 1911–1914 (2006).
[61] J. L. MacManus-Driscoll, P. Zerrer, H. Wang, H. Yang, J. Yoon, A. Fouchet, R. Yu, M. G. Blamire, and Q. Jia, Nat. Mater. **7**(4), 314–320 (2008).
[62] H. Yang, H. Wang, J. Yoon, Y. Wang, M. Jain, D. M. Feldmann, P. C. Dowden, J. L. MacManus-Driscoll, and Q. Jia, Adv. Mater. **21**(37), 3794–3798 (2009).
[63] S. A. Harrington, J. Zhai, S. Denev, V. Gopalan, H. Wang, Z. Bi, S. A. T. Redfern, S.-H. Baek, C. W. Bark, C.-B. Eom, Q. Jia, M. E. Vickers, and J. L. MacManus-Driscoll, Nat. Nanotechnol. **6**(8), 491–495 (2011).
[64] A. Imai, X. Cheng, H. L. Xin, E. A. Eliseev, A. N. Morozovska, S. V. Kalinin, R. Takahashi, M. Lippmaa, Y. Matsumoto, and V. Nagarajan, ACS Nano **7**(12), 11079–11086 (2013).
[65] T. Fix, E.-M. Choi, J. W. A. Robinson, S. B. Lee, A. Chen, B. Prasad, H. Wang, M. G. Blamire, and J. L. MacManus-Driscoll, Nano Lett. **13**(12), 5886–5890 (2013).
[66] A. Kursumovic, E. Defay, O. J. Lee, C.-F. Tsai, Z. Bi, H. Wang, and J. L. MacManus-Driscoll, Adv. Funct. Mater. **23**(47), 5881–5886 (2013).
[67] D. H. Kim, N. M. Aimon, X. Sun, and C. A. Ross, Adv. Funct. Mater. **24**(16), 2334–2342 (2014).
[68] W. Zhang, A. Chen, J. Jian, Y. Zhu, L. Chen, P. Lu, Q. Jia, J. L. MacManus-Driscoll, X. Zhang, and H. Wang, Nanoscale **7**(33), 13808–13815 (2015).
[69] A. Suwardi, B. Prasad, S. Lee, E.-M. Choi, P. Lu, W. Zhang, L. Li, M. Blamire, Q. Jia, H. Wang, K. Yao, and J. L. MacManus-Driscoll, Nanoscale **8**(15), 8083–8090 (2016).

[70] N. M. Aimon, D. H. Kim, H. K. Choi, and C. A. Ross, Appl. Phys. Lett. **100**(9), 092901 (2012).
[71] S.-C. Liao, P.-Y. Tsai, C.-W. Liang, H.-J. Liu, J.-C. Yang, S.-J. Lin, C.-H. Lai, and Y.-H. Chu, ACS Nano **5**(5), 4118–4122 (2011).
[72] A. Fouchet, H. Wang, H. Yang, J. Yoon, Q. Jia, and J. L. MacManus-Driscoll, IEEE Trans. Ultrason. Ferroelectrics Freq. Control **56**(8), 1534–1538 (2009).
[73] J. L. MacManus-Driscoll, A. Suwardi, A. Kursumovic, Z. Bi, C.-F. Tsai, H. Wang, Q. Jia, and O. J. Lee, APL Mater. **3**(6), 062507 (2015).
[74] Z. Bi, J. H. Lee, H. Yang, Q. Jia, J. L. MacManus-Driscoll, and H. Wang, J. Appl. Phys. **106**(9), 094309 (2009).
[75] J. S. Lee, S. B. Lee, B. Kahng, and T. W. Noh, Appl. Phys. Lett. **102**(25), 253503 (2013).
[76] S. Lee, J. S. Lee, J.-B. Park, Y. K. Kyoung, M.-J. Lee, and T. W. Noh, APL Mater. **2**(6), 066103 (2014).
[77] C. Korte, A. Peters, J. Janek, D. Hesse, and N. Zakharov, Phys. Chem. Chem. Phys. **10**(31), 4623–4635 (2008).
[78] S. Sanna, V. Esposito, A. Tebano, S. Licoccia, E. Traversa, and G. Balestrino, Small **6**(17), 1863–1867 (2010).
[79] D. Pergolesi, E. Fabbri, S. N. Cook, V. Roddatis, E. Traversa, and J. A. Kilner, ACS Nano **6**(12), 10524–10534 (2012).
[80] B. Li, J. Zhang, T. Kaspar, V. Shutthanandan, R. C. Ewing, and J. Lian, Phys. Chem. Chem. Phys. **15**(4), 1296–1301 (2013).
[81] J. Jiang, X. Hu, W. Shen, C. Ni, and J. L. Hertz, Appl. Phys. Lett. **102**(14), 143901 (2013).
[82] B. Yildiz, MRS Bulletin **39**(2), 147–156 (2014).
[83] Q. Su, D. Yoon, A. Chen, F. Khatkhatay, A. Manthiram, and H. Wang, J. Power Sources **242**, 455–463 (2013).
[84] E. Fabbri, D. Pergolesi, and E. Traversa, Sci. Technol. Adv. Mater. **11**(5), 054503 (2010).
[85] U. Aschauer, R. Pfenninger, S. M. Selbach, T. Grande, and N. A. Spaldin, Phys. Rev. B **88**(5), 054111 (2013).
[86] D. Pergolesi, E. Fabbri, A. D'Epifanio, E. Di Bartolomeo, A. Tebano, S. Sanna, S. Licoccia, G. Balestrino, and E. Traversa, Nat. Mater. **9**(10), 846–852 (2010).
[87] L. Sun, D. Marrocchelli, and B. Yildiz, Nat. Commun. **6**, 6294 (2015).
[88] S. H. Chang, S. C. Chae, S. B. Lee, C. Liu, T. W. Noh, J. S. Lee, B. Kahng, J. H. Jang, M. Y. Kim, D.-W. Kim, and C. U. Jung, Appl. Phys. Lett. **92**(18), 183507 (2008).
[89] S. H. Chang, J. S. Lee, S. C. Chae, S. B. Lee, C. Liu, B. Kahng, D.-W. Kim, and T. W. Noh, Phys. Rev. Lett. **102**(2), 026801 (2009).
[90] A. Chen, Z. Bi, C.-F. Tsai, J. Lee, Q. Su, X. Zhang, Q. Jia, J. L. MacManus-Driscoll, and H. Wang, Adv. Funct. Mater. **21**(13), 2423–2429 (2011).
[91] W. Zhang, A. Chen, Z. Bi, Q. Jia, J. L. MacManus-Driscoll, and H. Wang, Curr. Opin. Solid State Mat. Sci. **18**(1), 6–18 (2014).
[92] N. Schichtel, C. Korte, D. Hesse, and J. Janek, Phys. Chem. Chem. Phys. **11**(17), 3043–3048 (2009).
[93] D. Lee, A. Grimaud, E. J. Crumlin, K. Mezghani, M. A. Habib, Z. Feng, W. T. Hong, M. D. Biegalski, H. M. Christen, and Y. Shao-Horn, J. Phys. Chem. C **117**(37), 18789–18795 (2013).
[94] K. A. Stoerzinger, W. S. Choi, H. Jeen, H. N. Lee, and Y. Shao-Horn, J. Phys. Chem. Lett. **6**(3), 487–492 (2015).
[95] J. R. Petrie, H. Jeen, S. C. Barron, T. L. Meyer, and H. N. Lee, J. Am. Chem. Soc. **138**(23), 7252–7255 (2016).
[96] J. R. Petrie, C. Mitra, H. Jeen, W. S. Choi, T. L. Meyer, F. A. Reboredo, J. W. Freeland, G. Eres, and H. N. Lee, Adv. Funct. Mater. **26**(10), 1564–1570 (2016).
[97] J. R. Petrie, V. R. Cooper, J. W. Freeland, T. L. Meyer, Z. Zhang, D. A. Lutterman, and H. N. Lee, J. Am. Chem. Soc. **138**(8), 2488–2491 (2016).
[98] A. Fluri, D. Pergolesi, V. Roddatis, A. Wokaun, and T. Lippert, Nat. Commun. **7**, 10692 (2016).